Matter

CellPress

Article

Emerging materials and design principles for wurtzite-type ferroelectrics

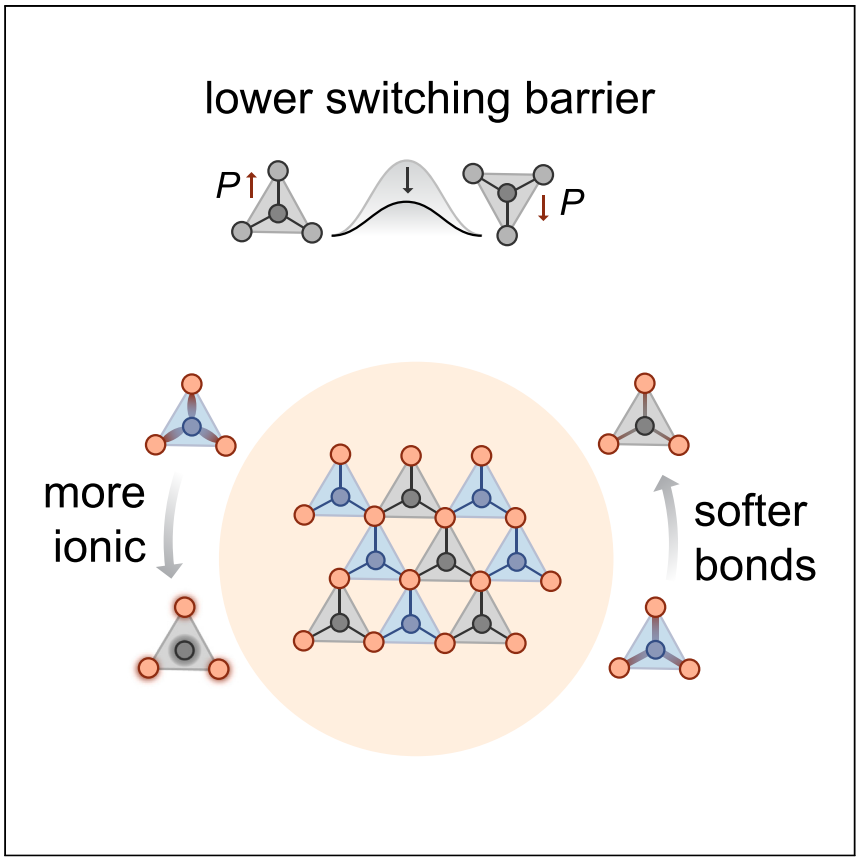

Wurtzite ferroelectrics such as (Al,Sc)N are promising for low-energy computing, but their switching electric fields are too high. Our computational search among multinary compounds finds four promising ternary nitrides and oxides for future experimentation. We identify unique switching pathways and non-polar intermediate structures. Our results show that the wurtzite *c*/*a* lattice parameter ratio is only valid within a given alloy and does not apply across different compounds. Instead, ionicity and bond strength emerge as effective design principles when comparing different chemistries.

Cheng-Wei Lee, Naseem Ud Din, Keisuke Yazawa, Geoff L. Brennecka, Andriy Zakutayev, Prashun Gorai

clee2@mines.edu (C.-W.L.)
pgorai@mines.edu (P.G.)

Highlights

Potential ferroelectric compounds identified with lower switching barriers than AlN

New switching mechanism described for multinary wurtzite-type ferroelectrics

Bond ionicity and softness identified as effective knobs to lower coercive field

1 **Discovery**
A new material or phenomena

Lee et al., Matter 7, 1–16
April 3, 2024
https://doi.org/10.1016/j.matt.2024.02.001

Please cite this article in press as: Lee et al., Emerging materials and design principles for wurtzite-type ferroelectrics, Matter (2024), https://doi.org/10.1016/j.matt.2024.02.001

Matter

CellPress

Article

Emerging materials and design principles for wurtzite-type ferroelectrics

Cheng-Wei Lee,[1,*] Naseem Ud Din,[1] Keisuke Yazawa,[1,2] Geoff L. Brennecka,[1] Andriy Zakutayev,[2] and Prashun Gorai[1,2,3,*]

SUMMARY

Low-energy compute-in-memory architectures promise to reduce the energy demand for computation and data storage. Wurtzite-type ferroelectrics are promising options for both performance and integration with existing semiconductor processes. The $Al_{1-x}Sc_xN$ alloy is among the few tetrahedral materials that exhibit polarization switching, but the electric field required to switch the polarization is too high (few MV/cm). Going beyond binary compounds, we explore the search space of multinary wurtzite-type compounds. Through this large-scale search, we identify four promising ternary nitrides and oxides, including Mg_2PN_3, $MgSiN_2$, Li_2SiO_3, and Li_2GeO_3, for future experimental realization and engineering. In >90% of the considered multinary materials, we identify unique switching pathways and non-polar structures that are distinct from the commonly assumed switching mechanism in AlN-based materials. Our results disprove the existing design principle based on the reduction of the wurtzite *c/a* lattice parameter ratio when comparing different chemistries while supporting two emerging design principles—ionicity and bond strength.

INTRODUCTION

With an increasingly digitized world, data centers and computing needs increase their energy consumption and carbon footprint.[1,2] The computational share of energy consumption in the last decade plateaued at about 1% of global energy consumption, thanks to improvements in efficiency and adoption of cloud computing.[3] However, these improvements are expected to reach their limit soon,[3,4] while growth in data centers and computing needs is expected to continue.[5] Therefore, breakthroughs in energy-efficient computing, data storage, and communication are critical for minimizing the associated environmental impacts.

Ferroelectrics maintain a spontaneous electric polarization without the need for constant external energy, and the direction of this polarization can be switched on demand via the application of an electric field. These two key features make ferroelectrics promising materials for energy-efficient data storage in comparison to dynamic random access memory[6] and for neuromorphic computing and related memory-logic hybrids, which need simultaneous and colocated data storage and information processing.[7–9] Recently discovered tetrahedral (wurtzite-type) ferroelectrics are of particular interest because of the relative ease of direct and high-quality integration with existing and emerging tetrahedral semiconductors (e.g., Si, GaAs, GaN, SiC, AlN).[6,10]

PROGRESS AND POTENTIAL

Low-energy compute-in-memory architectures promise to reduce the global energy demand for computation and data storage. Wurtzite-type ferroelectrics such as (Al,Sc)N alloy offer advantages over current devices in both performance and integration with existing semiconductor processes, but at present, all known wurtzite-type ferroelectrics require excessively large operating voltages for polarization reversal. We report a large-scale computational search among multinary compounds for new materials with polarization-switching barriers lower than AlN while maintaining large breakdown fields. Four ternary nitrides and oxides are identified as candidates for future experimentation. We also identify unique switching pathways and non-polar structures. Our results show that the existing design principle based on the reduction of the wurtzite *c/a* lattice parameter ratio does not apply when comparing different compounds. Instead, ionicity and bond strength emerge as effective design principles.

Please cite this article in press as: Lee et al., Emerging materials and design principles for wurtzite-type ferroelectrics, Matter (2024), https://doi.org/10.1016/j.matt.2024.02.001

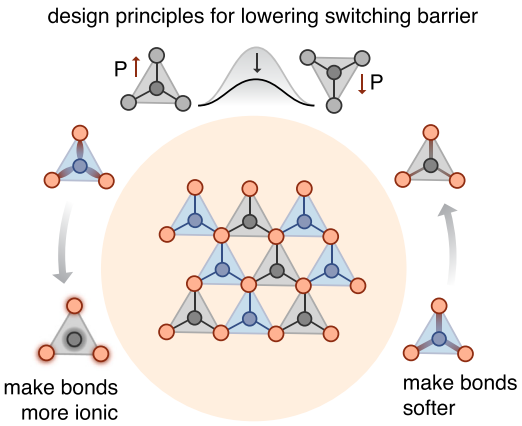

Figure 1. Design principles for wurtzite-type ferroelectrics
Emerging design principles for discovery and engineering of multinary tetrahedral (wurtzite-type) ferroelectrics with lower coercive fields. More ionic and softer bonds lower polarization switching barriers.

It has long been recognized that wurtzite-type structures possess very large spontaneous polarization, often >100 μC/cm^2,[11] but it was not until Fichtner et al. demonstrated in 2019 that the polarization of $Al_{1-x}Sc_xN$ could be reversed under an applied electric field prior to dielectric breakdown[10] that tetrahedrally bonded materials were acknowledged as potentially ferroelectric. In recent years, robust ferroelectricity has also been demonstrated in $Al_{1-x}B_xN$, $Ga_{1-x}Sc_xN$, and $Zn_{1-x}Mg_xO$ alloys.[12–15] The large spontaneous polarization values of these tetrahedrally bonded ferroelectrics are of interest for neuromorphic architectures and open up the possibility of multistate bits,[16,17] but the coercive fields—and therefore switching voltages—are still one to two orders of magnitude higher than ideal.[18]

A variety of techniques, e.g., higher substitution, tensile strain, and elevated temperatures, have been shown to reduce the coercive field of the AlN-based alloys.[10,13,14,19–24] Here, we adopt a complementary approach to computationally identify new multinary wurtzite-type compounds with similar or lower switching barriers to AlN and ZnO, presuming that these candidates will also be further improved via alloying, strain engineering, etc. The idea is to identify new materials with suitable initial properties (low barrier for switching and large breakdown field) before further engineering. In comparison to previous computational searches,[18,25] we expand the search space and focus on multinary ($n > 2$, where n is the number of chemical elements) wurtzite-type compounds.

To identify suitable candidates in a computationally accessible manner, we utilized the intrinsic breakdown field (E_b) and switching barrier (ω_s) in single crystals as search parameters. The actual dielectric breakdown and ferroelectric switching mechanisms are expected to be more complicated based on contributions from impurities, defects, field inhomogeneities, etc.,[26,27] but the calculated E_b and ω_s represent their respective upper limits. Therefore, ω_s and E_b provide the relative tendencies to switch and to experience breakdown among different candidates. With these two calculated material properties and using AlN as the reference material, we identified several candidates that should demonstrate polarization switching before dielectric breakdown, and the most promising ones are Mg_2PN_3, Li_2SiO_3, Li_2GeO_3, and $MgSiN_2$. We identify unique switching pathways and intermediate non-polar structures for multinary (ternary and above) compounds. These pathways are distinct from the commonly assumed wurtzite-hexagonal-wurtzite switching pathway for binary compounds in the literature.[11,28–30] Furthermore, our calculated results of switching barriers provide systematic evidence across different chemistries for two qualitative design principles—ionicity and bond strength (Figure 1). These

[1]Metallurgical and Materials Engineering, Colorado School of Mines, Golden, CO 80401, USA

[2]Materials Science Center, National Renewable Energy Laboratory, Golden, CO 80401, USA

[3]Lead contact

*Correspondence: clee2@mines.edu (C.-W.L.), pgorai@mines.edu (P.G.)

https://doi.org/10.1016/j.matt.2024.02.001

Please cite this article in press as: Lee et al., Emerging materials and design principles for wurtzite-type ferroelectrics, Matter (2024), https://doi.org/10.1016/j.matt.2024.02.001

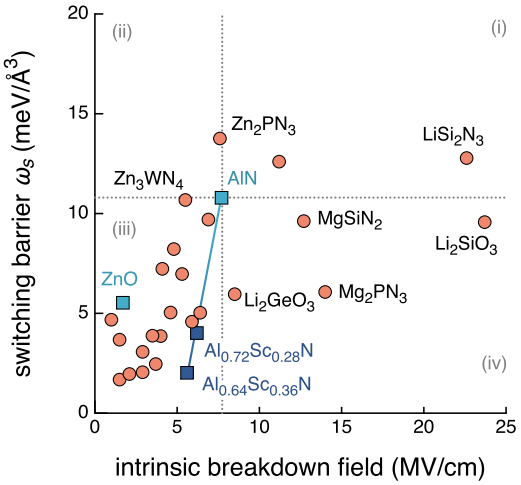

Figure 2. Candidate wurtzite-type ferroelectric materials

Comparing calculated switching barriers (ω_s) to intrinsic dielectric breakdown fields of 24 candidates and 2 references compounds (AlN and ZnO). Values for $Al_{1-x}Sc_xN$ alloys (x = 0.28, 0.36) are also shown for reference. Sc substitution in AlN decreases ω_s almost linearly with x. ω_s values for $Al_{1-x}Sc_xN$ are taken from Lee et al.[33]

fundamental materials knobs can be tuned for future materials discovery and further engineering of candidates to have lower switching barriers and thus lower coercive fields.

RESULTS AND DISCUSSION

Candidate materials with low switching barriers and high breakdown fields

The defining feature of ferroelectricity is that the spontaneous polarization needs to be switchable under an applied electric field.[10,31] The major challenge that prevents wurtzite-type ferroelectrics—or any polar material—from being switchable is that increasing electric field can cause dielectric breakdown before switching. To a first order, the coercive field is proportional to the switching barrier in units of energy density.[32] Therefore, we perform a computational search for candidates with higher intrinsic dielectric breakdown fields (E_b) and lower switching barriers (ω_s) than reference wurtzite materials like AlN and ZnO. Pure AlN and ZnO are not ferroelectrics at room temperature, but they represent materials that have the potential to be—in fact, have been—further engineered, e.g., via alloying.[12–15]

Specifically, what distinguishes our work from previous computational searches[18,25] is that we used the solid-state nudged elastic band (SS-NEB) method to calculate the switching barrier and that we estimate the E_b, which is a critical property for ferroelectrics. The SS-NEB method is known to predict lower and more physical switching barriers than the traditional NEB method since it allows more degrees of freedom, i.e., allows changes in cell volume and shape.[32] Moreover, our search focuses on multinary wurtzite-type compounds and includes sulfides and selenides in addition to nitrides and oxides, which allows us to deduce more general design principles that are applicable across chemistries.

Within a search space of 399 tetrahedral structures from the Inorganic Crystal Structure Database (ICSD), we identified 117 wurtzite-type structures (see experimental procedures for details). Figure 2 compares the E_b and ω_s of 24 multinary candidates that have thermodynamically stable wurtzite-type structures with c/a values less than 1.603 (AlN c/a). We also included AlN and ZnO as reference materials and 9 newly discovered wurtzite-type nitrides[34] where the c/a criterion was not imposed. For the switching barrier, instead of the commonly used unit of eV/f.u., we used eV/Å^3

Please cite this article in press as: Lee et al., Emerging materials and design principles for wurtzite-type ferroelectrics, Matter (2024), https://doi.org/10.1016/j.matt.2024.02.001

for the following reasons. First, the coercive field depends on the energy density (eV/Å^3) directly.[31] Moreover, when comparing multinary compounds with different stoichiometries, the choice of the unit of eV/f.u. overestimates the barriers for compounds with higher numbers of atoms per f.u. and thus leads to qualitatively different rankings (see Figure S1 in comparison to Figure 2).

From a bird's eye view, Figure 2 shows that wurtzite-type compounds with larger E_b generally have larger switching barriers. Such a correlation showcases the difficulty of searching for candidates with lower switching barriers but higher E_b. Fortunately, for compounds with similar E_b, their ω_s can still vary by two to three times. This observation makes the search possible and suggests that factors other than E_b (which predominately depends on the electronic band gap) may be important for the switching barrier.

Using AlN as a baseline, there are four quadrants regarding the likelihood to demonstrate polarization switching: (1) higher E_b and higher ω_s, (2) lower E_b and higher ω_s, (3) lower E_b and lower ω_s, and (4) higher E_b and lower ω_s. Figure 2 shows that there are a few oxides (Li_2SiO_3 and Li_2GeO_3) and nitrides ($MgSiN_2$ and Mg_2PN_3) within quadrant 4, which is the search target region and the quadrant with the highest likelihood of polarization switching. In comparison, Zn_2PN_3 in quadrant 2 has the lowest likelihood of demonstrating polarization switching due to a combination of a larger switching barrier and a lower breakdown field than AlN.

Compounds in quadrants 1 and 3 are also potential candidates as demonstrated by ZnO (in quadrant 3) and, particularly, by the $Zn_{1-x}Mg_xO$ alloy and our recent results for $Al_{1-x}Sc_xN$ alloys.[33,35] $LiSi_2N_3$ in quadrant 1 has slightly larger ω_s (by ~2 meV/Å^3), but its E_b is almost three times the estimated value for AlN. Generally speaking, for compounds within quadrants 1 and 3, we expect increasing likelihood to demonstrate polarization switching with closer proximity to the search target region. Overall, the broader search space leads to a large set of multinary compounds that can have higher E_b and lower ω_s than baseline materials like AlN and ZnO. We note that some of the top candidates contain Li ions, which are known fast-diffusing species in Si and can form Li-Si phases.[36] This can lead to potential Li contamination and irreducible damage to a Si-based device. While the contamination can be mitigated by diffusion barrier layers, such limitation makes non-Li-containing candidates more promising for future applications.

Lastly, we compare the candidate compounds to ferroelectric $Al_{1-x}Sc_xN$ alloys. Figure 2 shows that none of the multinary compounds simultaneously have lower switching barriers and higher E_b than $Al_{1-x}Sc_xN$ alloys. This suggests that the top candidates will likely require further engineering, such as alloying, to demonstrate polarization switching.

Existing design principle for switching barriers

Previous studies on wurtzite-type alloy ferroelectrics support the wurtzite *c*/*a* lattice parameter ratio as a key empirical descriptor for switching behavior in wurtzite-type ferroelectrics—the lower the *c*/*a* value, the lower the switching barrier (coercive field).[10,24] However, recent works have started to challenge its validity. We have recently identified the importance of ionicity of metal–anion bonds for describing the switching barrier in wurtzite-type ferroelectrics.[21] Recent studies have shown that the coercive field decreases with increasing B concentration in $Al_{1-x}B_xN$ alloy, while the wurtzite *c*/*a* values are independent of the B concentration.[12] Similar findings have been reported for $Zn_{1-x}Mg_xO$ alloy, where *c*/*a* remains constant. Since

Please cite this article in press as: Lee et al., Emerging materials and design principles for wurtzite-type ferroelectrics, Matter (2024), https://doi.org/10.1016/j.matt.2024.02.001

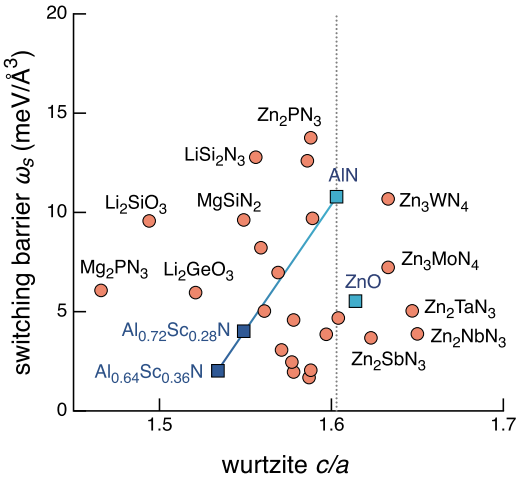

Figure 3. Validity of known design rules

Calculated switching barrier (ω_s), based on SS-NEB energy barrier, for 24 candidates and 2 reference compounds (AlN and ZnO). Values for $Al_{1-x}Sc_xN$ alloys (x = 0.28, 0.36) are also shown for reference. Sc substitution in AlN decreases *c/a* almost linearly with *x*. The vertical dashed line indicates the AlN wurtzite *c/a* value of 1.603. ω_s is correlated with wurtzite *c/a* lattice parameter ratio for $Al_{1-x}Sc_xN$ alloys but not for compounds across different chemistries.

these studies focus only on alloys derived from AlN or ZnO, the generalizability of the wurtzite *c/a* value as a universal predictor remains unclear.

Since our computational search space includes multinary compounds and is not limited to the ideal wurtzite structure, our results provide a great opportunity to examine the validity of the wurtzite *c/a* value as a predictor for switching barrier. Our computational search for multinary wurtzite-type compounds with lower switching barriers still utilizes the wurtzite *c/a* as a descriptor due to its historical importance mentioned above and in order to have a manageable amount of candidates for computationally intensive switching barrier calculations. The barriers are then calculated with the generalized SS-NEB method (see experimental procedures), and the results allow us to examine the validity of this established design principle.

Figure 3 shows the relationship between switching barrier and wurtzite *c/a* value for 2 reference binary wurtzite materials (AlN and ZnO) and 24 candidates. Values for $Al_{1-x}Sc_xN$ alloys (x = 0.28, 0.36) are also shown in Figure 3 for added reference. We calculate the wurtzite *c/a* value based on density functional theory (DFT)-relaxed structures and the group-subgroup symmetry relations discussed by Breternitz et al.[37] Consistent with previous experimental measurements, our results show that alloying AlN with Sc reduces *c/a* values and switching barriers almost linearly.[10] However, Figure 3 clearly shows that there is no significant correlation between switching barrier and wurtzite c/a for compounds across different chemistries. Using AlN as a reference point, the switching barrier can either increase or decrease with smaller *c/a* values. Therefore, our results show that the wurtzite *c/a* lattice parameter ratio is not a good descriptor of switching barriers across different chemistries. It is worth noting that the *c/a* value remains a practical descriptor for engineering a single compound via alloying since *c/a* generally correlates with local bond ionicity and ionic displacement, which are the emerging design principles for switching barriers.[21] Further discussion can be found in the following section.

Emerging design principles for switching barriers

The results in Figure 3 not only disprove the wurtzite *c/a* value as a good descriptor across different chemistries for switching barrier but also support two emerging design principles—ionicity and bond strength. Figure 4 demonstrates the principles by comparing compounds of the same chemistry group but with cations of different electronegativities. Figure 4 still supports the correlation between the wurtzite *c/a*

Please cite this article in press as: Lee et al., Emerging materials and design principles for wurtzite-type ferroelectrics, Matter (2024), https://doi.org/10.1016/j.matt.2024.02.001

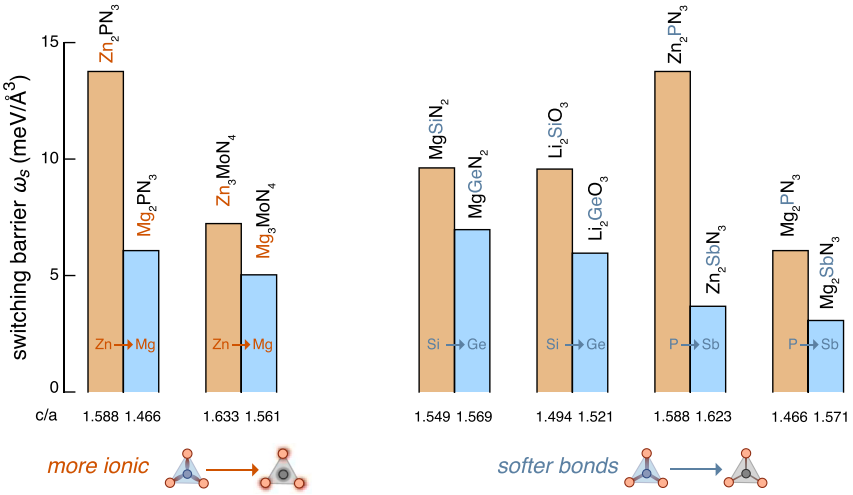

Figure 4. Materials design principles for lowering switching barrier

Switching barrier (ω_s) of materials pairs selected to demonstrate the two emerging design principles—bond ionicity and softness. More ionic cation–anion bonds (e.g., Zn → Mg) reduce ω_s, while softer and more polarizable cation–anion bonds (e.g., P → Sb) also lead to reduced ω_s. However, bond ionicity and softness are not completely independent materials properties (Figure S3).

value and switching barrier within certain chemistry groups. Using Zn_2PN_3 and Mg_2PN_3 and Zn_3MoN_4 and Mg_3MoN_4 as example pairs, smaller *c/a* values correlate with smaller switching barriers. However, we want to emphasize that the *c/a* value is not the cause but rather the consequence of local bond ionicity.[21] In other words, it is the more ionic nature of Mg–N bonds than Zn–N bonds that gives rise to lower switching barriers (and lower *c/a* values) for wurtzite-type candidates containing Mg than the ones with Zn (Figure 4).

Figure 3 also shows that softer chemical bonds can lead to smaller switching barriers. Overall, sulfides and selenides, which generally form softer (more polarizable) bonds than oxides and nitrides, have lower switching barriers. This is consistent with the chemical intuition that cations move more easily and that atomic volumes are larger for materials with softer chemical bonds. Besides, with two nominal cations in ternary wurtzite-type compounds, the same trend can be seen for, e.g., Zn_2MN_3 chemistry (M = P, Sb, Nb, Ta). Sb, Nb, and Ta, which generally form softer cation–N bonds than P, give rise to smaller switching barriers (Figure 4). Similarly, $MgGeN_2$, $LiGe_2N_3$, and Li_2GeO_3 have lower switching barriers than $MgSiN_2$, $LiSi_2N_3$, and Li_2SiO_3, respectively, which is consistent with the chemical intuition that Ge forms more polarizable bonds with O and N atoms than Si. Interestingly for these chemical substitutions, we find that smaller *c/a* values actually correlate with larger switching barriers. This supports the limited applicability of *c/a* as a descriptor for switching barrier.

To achieve the engineering goal of enabling ferroelectric switching in wurtzite-type compounds, we need not only low switching barriers but also sufficiently high dielectric breakdown fields, which predominantly depends on the electronic band gap (see experimental procedures). Therefore, we further qualitatively examined how these two design principles affect the electronic band gap and the indication for dielectric breakdown field. Using the known $Zn_{1-x}Mg_xO$ system as an example, Mg–O bonds are more ionic than Zn–O bonds, and at the same time, MgO has a larger electronic band gap. As a result, alloying ZnO with MgO leads to smaller

Please cite this article in press as: Lee et al., Emerging materials and design principles for wurtzite-type ferroelectrics, Matter (2024), https://doi.org/10.1016/j.matt.2024.02.001

coercive fields and larger band gaps.[35] In comparison, for $Al_{1-x}Sc_xN$, even though Sc–N bonds are more ionic than Al–N bonds,[21] rock-salt ScN has a relatively small band gap of ~1 eV.[38] Therefore, alloying leads to not only smaller coercive fields but also smaller band gaps. Based on these observations, one can engineer a compound further via alloying it in a way that lowers the switching barrier and enhances the breakdown field. The ideal alloying strategy is to substitute cations with same-valency (oxidation state) cations that form more ionic bonds with the anion.

From the bond strength perspective, since softer materials generally have smaller band gaps, exemplified by comparing selenides and sulfides to oxides, careful trade-off is needed to avoid a significant decrease in electronic band gaps and, therefore, reduction in breakdown fields. Furthermore, bond ionicity and strength are not fully independent materials properties. Figure S3 compares the switching barrier of the material pairs in Figure 4 as a function of their bulk modulus, which is a measure of bond strength. Changing bond ionicity will simultaneously affect bond softness and band gap, with the latter directly affecting the breakdown field. Therefore, how to balance the switching barrier and dielectric breakdown field remains highly non-trivial, and a descriptor that can simultaneously correlate with a smaller switching barrier and a larger electronic band gap is desirable for future investigations.

New switching mechanism and non-polar structure

The current understanding of polarization switching in tetrahedral ferroelectrics is largely based on studies on wurtzite-type alloys derived from AlN[10,32,39] and ZnO,[35] in which the switching is assumed to proceed via the wurtzite-hexagonal BN-like (hBN)-wurtzite pathway, as shown in Figure 5A, under an external electric field.[11,28–30]

But a recent computational study,[40] which uses the NEB method, on $Al_{1-x}B_xN$ identified a switching mechanism that undergoes a pathway in which the β-BeO-like structure is the non-polar intermediate structure. Unlike the commonly assumed non-polar hBN-like structure, which is a saddle point in the transformation pathway, this β-BeO structure is a local minimum along the pathway (metastable). Recent experimental evidence suggests that $Al_{1-x}B_xN$ reverses polarity via non-polar intermediate structures that are also not the hBN-like structure during switching.[41] Instead, the intermediate structure is an average non-polar, metastable structure consisting of anti-polar arrangements of wurtzite motifs when viewed along the [100] direction. Among other things, these findings could suggest that increasing chemical complexity (beyond binary wurtzites) can lead to different switching pathways, but this idea requires further investigation.

Multinary wurtzite-type ordered compounds share some similarity with AlN-based alloys in such a way that cations with different ionicities and radii cause distortion from an ideal wurtzite structure and give rise to different potential energy landscapes. For the 24 multinary candidates studied here, only two of them, $ZnTiN_2$ and Mg_3MoN_4, follow the commonly assumed wurtzite-hBN-wurtzite switching pathway. In comparison, we find that the rest of the 22 wurtzite-type compounds follow a new switching pathway, shown in Figure 5B. We use $LiGaSe_2$, which has the lowest switching barrier, as an example to demonstrate the new pathway, but the same feature as detailed below applies to all 22 candidates.

Before proceeding, we must define a consistent terminology to aid our explanation. Since all of the compounds in this study have a single anion and multiple cations, we

Please cite this article in press as: Lee et al., Emerging materials and design principles for wurtzite-type ferroelectrics, Matter (2024), https://doi.org/10.1016/j.matt.2024.02.001

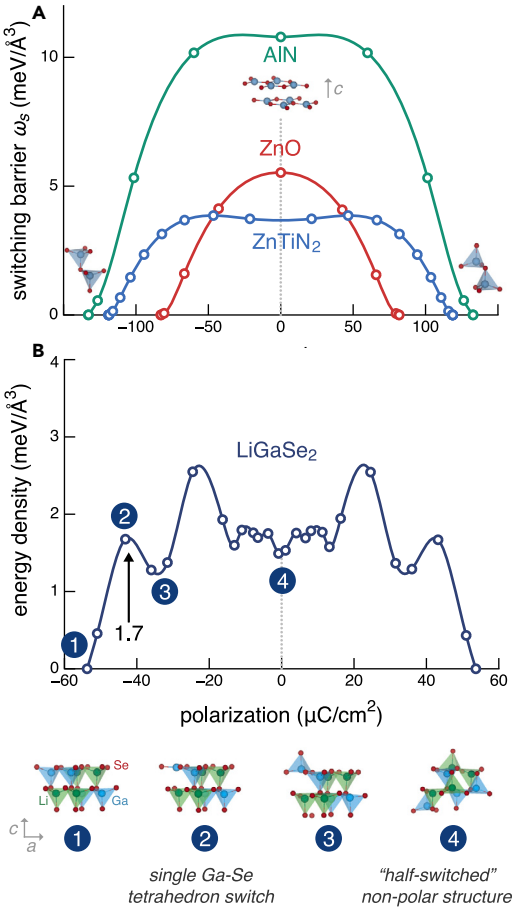

Figure 5. Polarization switching mechanisms

Switching barrier (ω_s) as a function of polarization for two switching mechanisms. Solid curves are cubic spline fits to the data points obtained from SS-NEB calculations. The switching barriers are indicated by arrows for ZnO and $LiGaSe_2$.

(A) Collective switching: AlN and ZnO, which are the baseline materials, are used to demonstrate collective switching. The intermediate hBN-like structure of AlN is shown as the inset. $ZnTiN_2$ is a ternary compound that exhibits collective switching.

(B) $LiGaSe_2$, which has the lowest switching barrier, is used to demonstrate the individual switching mechanism. Crystal structures along the switching pathway are shown, including the half-switched non-polar intermediate structure.

define the tetrahedral structural unit ("wurtzite motif" in Calderon et al.[41]) according to the cation. Thus, when we say that a cation tetrahedron is oriented "up," that means the polarization axis is vertical (along [001]) and that the nearest anion that sits directly on the axis with the cation is above the cation; if the same tetrahedron were oriented "down," then the cation would be below the anion basal plane, and the nearest c axis-aligned anion would be below this cation.

The key differences of the new pathways from the wurtzite-hBN-wurtzite pathway lie not only in the non-polar intermediate structures but also the atomic-scale switching processes. Unlike the known hBN-like non-polar structure, new non-polar structures that the SS-NEB method identifies using the primitive cell have half of the cation tetrahedra of the same type pointing in one direction along the polarization axis while the other half point in the opposite direction (crystal structures in Figure 5B). Among these new non-polar structures, some (e.g., $LiGaSe_2$ in Figure S2)

Please cite this article in press as: Lee et al., Emerging materials and design principles for wurtzite-type ferroelectrics, Matter (2024), https://doi.org/10.1016/j.matt.2024.02.001

share similarity with the β-BeO structure recently identified,[40,41] while some are completely new (e.g., $LiAlS_2$ in Figure S2). In all these structures, since half of the cation tetrahedra are switched and, on average, have net zero polarization, we refer to them as "half-switched structures" (Figure 5B). The half-switched structures are metastable, i.e., located in potential energy wells. The structures along the transformation pathway, including the new non-polar structures, are available on GitHub.[42]

Figure 5 also shows distinct switching processes between the known and new switching pathways. All the cation tetrahedra switch coherently at the same time for the known wurtzite-hBN-wurtzite pathway, while individual cation tetrahedra switch sequentially for the new pathway. Therefore, we refer to the known and new pathways as collective and individual switching, respectively, for the rest of the article. The difference in pathways affects how the switching barriers are calculated. For collective switching, the barrier is either the energy density difference between the wurtzite-type polar structure and the hBN-like non-polar structure (AlN and ZnO in Figure 5A) or the maximal energy density difference along the transformation pathway when the hBN-like non-polar structure is not the highest energy structure ($ZnTiN_2$ in Figure 5A). However, for individual switching, the switching barrier is the largest barrier defined by a valley and its adjacent peak toward the switching direction. The idea is that if an applied electric field is large enough to overcome the largest barrier, then it is large enough to overcome all of the other barriers.

Overall, the prevalence of materials that follow some version of a new switching pathway (individual switching in 22 out of 24 multinary compounds) supports the hypothesis that increased chemical complexity can lead to different switching pathways and reduced overall switching barriers. Further investigations into the underlying mechanisms are clearly needed but are beyond the scope of this manuscript.

Further considerations

We acknowledge that the calculated switching barriers are only the upper limit for the actual switching mechanisms, as they do not account for domain wall motion or any effects of defects. This limitation is known in the literature,[32,43] but we emphasize that the goal is not to quantitatively predict the coercive field but to qualitatively examine the required energy density to switch polarization. We also note that it is only very recently that domain walls have even been confirmed in these ferroelectric wurtzites[7] and that both the structures of the imaged domain walls and the relatively low energy of intermediate states via the individual switching pathways we report here would represent incredibly high-charge-density structures according to classic domain wall models.[31,44] Thus, there is a clear need for additional study of domain walls in tetrahedral ferroelectrics.

Our DFT calculations represent switching barriers at zero temperature, but switching barriers are known to decrease with increased temperature experimentally[13,24] and theoretically.[31,32] On the other hand, increasing temperature has mixed effects on dielectric breakdown fields since higher temperature generally gives rise to smaller electronic band gaps but to stronger electron-phonon interactions, which help dissipate energy delivered via electric field.[45] Recent experimental observations in $Al_{0.84}Sc_{0.16}N$, $Al_{0.93}B_{0.07}N$, and AlN thin films show decreasing breakdown fields with increasing temperature, but their temperature dependency is significantly weaker than that of coercive field.[24] Therefore, just as was the case in experiments, we expect the margin between coercive and breakdown fields to increase with increased temperature and, therefore, for the trends identified here to be the same or possibly exaggerated at finite temperatures.

Please cite this article in press as: Lee et al., Emerging materials and design principles for wurtzite-type ferroelectrics, Matter (2024), https://doi.org/10.1016/j.matt.2024.02.001

Conclusions

In summary, we performed a computational search and identified novel wurtzite-type compounds that can integrate with existing tetrahedrally bonded semiconductors while exhibiting sufficiently small coercive fields. Utilizing crystal symmetry relationships among wurtzite and its derived structures, we focus on the search space of wurtzite-type multinary compounds, which extends previous searches on binary wurtzite structures both in chemistry and complexity. Using AlN as a reference, we found that the larger search space opens up an opportunity to find new wurtzite-type materials with smaller switching barriers while maintaining or even increasing intrinsic dielectric breakdown fields. Specifically, we find that Mg_2PN_3, Li_2SiO_3, Li_2GeO_3, and $MgSiN_2$ are the most promising wurtzite-type compounds for future investigations. With switching barriers calculated by the SS-NEB method for 24 multinary wurtzite-type compounds, we find that wurtzite *c/a* values have no significant correlation with switching barriers across different chemistries but could remain a useful descriptor of switching barriers within certain chemistry groups. Instead, our results support two emerging design principles to achieve lower switching barriers—higher ionicity and lower bond strength. Between them, ionicity can be a more promising parameter for future engineering of candidates, e.g., via alloying, since higher ionicity generally gives rise to larger electronic band gaps, while softer materials generally have smaller band gaps. Lastly, we find that the majority (>90%) of the multinary wurtzite-type candidates prefer different switching pathways that go through new non-polar, metastable structures. Overall, further understanding of the underlying switching mechanisms, along with the two design principles identified here, has the potential for discovering and engineering multinary wurtzite-type ferroelectrics, which are promising for next-generation low-power computing.

EXPERIMENTAL PROCEDURES

Resource availability

Lead contact

Further information and requests for data should be directed to and will be fulfilled by the lead contact, Prashun Gorai (pgorai@mines.edu).

Materials availability

This study did not generate new unique materials.

Data and code availability

Structures along the polarization pathway determined by SS-NEB calculations are available on GitHub.[42] This paper does not report original code.

Computational search workflow

The goal of the computational search was to find new wurtzite-type compounds that can have low switching barriers but high E_b. A schematic of the computational workflow is shown in Figure 6. We performed a search for stoichiometric and ordered tetrahedrally bonded structures (TBSs) from the ICSD. The TBSs were identified using an automated procedure where the coordination was calculated by determining the first nearest neighbors using the minimum distance approach with a tolerance of 0.3–0.5 Å. Each atom in a TBS must have 4-fold coordination. Next, we checked to ensure that the tetrahedral bond angles are within $109.5^\circ \pm 20^\circ$. The large tolerance (20°) on the bond angles accommodates the distorted tetrahedral structures. This procedure for identification of TBSs is similar to the one we used in Gorai et al.[46] We identified 399 TBSs spanning binary (153), ternary (127), and quaternary (119) chemistries. We also considered 9 newly discovered wurtzite-type nitrides,[34] some of which have been experimentally synthesized.[47] We utilized the known

Please cite this article in press as: Lee et al., Emerging materials and design principles for wurtzite-type ferroelectrics, Matter (2024), https://doi.org/10.1016/j.matt.2024.02.001

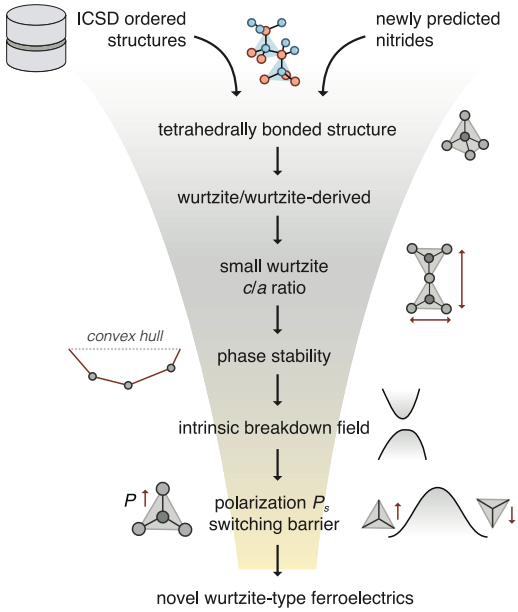

Figure 6. Computational search workflow

Schematic of the computational workflow to identify novel wurtzite-type ferroelectric materials.

group-subgroup symmetry relations[37] to identify 117 wurtzite-type structures out of the 399 TBSs.

Motivated by the empirical observation that a lower wurtzite *c*/*a* lattice parameter ratio leads to smaller coercive fields, we prescreened the 117 wurtzite-type structures from the ICSD to identify initial candidates with *c*/*a* <1.603 (AlN *c*/*a*). We should note here that we ultimately find that wurtzite *c*/*a* is not a good descriptor for switching barriers across different chemistries.

Next, we assessed the thermodynamic phase stability of the wurtzite-type structures through convex hull analysis. We considered competing phases from the ICSD to construct the convex hull. In most cases, the total energy of the competing phases were taken from the NREL Materials Database.[48] DFT relaxations of the remaining structures were performed with the plane-wave Vienna Ab initio Simulation Package (VASP) code[49] using the Perdew-Burke-Ernzerhof exchange correlation functional within the generalized gradient approximation (GGA).[50] The valence electrons were treated with the projector-augmented wave method. A plane-wave energy cutoff of 340 eV was used, and automatically generated Γ-centered Monkhorst-Pack *k*-point grids were used to sample the Brillouin zone. The formation enthalpy of the wurtzite-type structures and competing phases was calculated from their DFT total energy and reference chemical potentials of the elemental phases. We used the fitted elemental-phase reference energies as the reference chemical potentials, which have been shown to provide accurate predictions of formation enthalpy.[51] At the end, we downselected 24 wurtzite-type materials, including 9 new nitrides.

In the final step of the computational workflow, we employed a phenomenological model to estimate the E_b[52] and the SS-NEB method to calculate the polarization switching pathways and energy barriers.[53] Through this computational search, we identified four promising wurtzite-type ternary compounds as candidates with lower switching barriers and higher E_b compared to AlN.

Please cite this article in press as: Lee et al., Emerging materials and design principles for wurtzite-type ferroelectrics, Matter (2024), https://doi.org/10.1016/j.matt.2024.02.001

Intrinsic breakdown field

We used a phenomenological model developed by Kim et al.[52] to estimate the intrinsic dielectric breakdown field E_b (in MV/m):

$$E_b = 24.442\ exp\left(0.315\sqrt{E_g\omega_{max}}\right), \qquad \text{(Equation 1)}$$

where ω_{max} is the maximum phonon frequency (in THz) at the Γ point of the Brillouin zone and E_g is the band gap (in eV). Semi-local DFT functionals are known to severely underestimate E_g. To address this issue, we calculated E_g of the candidate materials with the DFT hybrid functional HSE06,[54] which generally provides a better prediction of E_g. First, we relaxed the candidate wurtzite-type structures with the HSE06 functional using the default 25% exchange fraction. Then, we calculated the electronic band structures, also with the HSE06 functional, on a dense k-point grid such as $N \times n_{kpts} \simeq 8000$, where N is the number of atoms in the primitive cell and n_{kpts} is the number of k-points. For reference, a k-point density of 8,000 translates to a 14 × 14 × 14 k-point grid for the Si primitive cell. Future in-depth studies of specific candidate materials may employ a beyond-DFT method such as the GW approximation for even more accurate E_g predictions.

Spontaneous polarization

We followed the modern theory of polarization,[55,56] which uses the Berry phase approximation to calculate the electronic contribution to polarization. Specifically, we used the VASP 5.4.4. implementation and chose (0.25, 0.25, 0.25) crystal coordinates as the center of the reference frame for dipole calculations. The numerical parameters discussed in "Computational search workflow" were used for the Berry phase calculations. To calculate the ionic contribution to polarization, we used the atomic positions and assumed point charges; the calculation implemented in Pymatgen was used.[57] After the switching pathways were determined with the SS-NEB method, we used the algorithm implemented in Pymatgen to identify smooth polarization pathways and to calculate the polarization quanta.[57] In each case, we visually checked the smoothness of the polarization pathway since the automated algorithm in Pymatgen fails in certain cases.[57] In such cases, we manually identified smooth polarization pathways.

Switching pathway and energy barrier

We applied the SS-NEB method[53] to determine the switching pathways between the polar and anti-polar structures and to calculate the switching energy barrier (ω_s) along the pathways. We performed SS-NEB calculations using VASP Transition State Theory (VTST) tools developed by Henkelman and Jonsson.[58] Specifically, VASP (VASP 5.4.4) and vtstcode-182 were used. First, we relaxed the polar wurtzite-type structure with DFT. We then created the anti-polar structure by applying mirror reflection to the relaxed polar structure. By design, the anti-polar structure is relaxed and does not require further DFT relaxation. We created intermediate images through linear interpolation between the relaxed polar and anti-polar structures. Generally, such linear interpolation generates the common switching pathway via an hBN non-polar structure. This linearly interpolated pathway is qualitatively similar to the converged SS-NEB pathways shown in Figure 5A. We found that when the switching occurs via the hBN structure, SS-NEB calculations require only a small number of intermediate images (<10) for convergence (forces < 10^{-2} eV/Å). However, convergence of more complex switching pathways, such as the one shown for $LiGaSe_2$ in Figure 5B, requires a large number of intermediate images—roughly 2–8 times the number of cations in the simulation cell. As a result, SS-NEB calculations for the latter are computationally expensive but more accurate in unveiling

Please cite this article in press as: Lee et al., Emerging materials and design principles for wurtzite-type ferroelectrics, Matter (2024), https://doi.org/10.1016/j.matt.2024.02.001

unique switching mechanisms and non-polar intermediate structures. Lastly, since SS-NEB calculations allow cell degrees of freedom (similar to DFT structure relaxation), it is critical to update the Fourier grid after a certain number of ionic steps and to use a large plane-wave cutoff energy for accurate calculation of stress and convergence of SS-NEB calculations. From the converged switching pathway, we determined the switching barrier as the largest among the individual barriers along the pathway. The switching barrier is normalized by cell volume and is reported in eV/Å^3.

The interpretation of the switching barrier for the individual mechanism and its comparison to the switching barrier for collective mechanism warrants further discussion. Our approach is conceptually similar to that used in Calderon et al.[41] The NEB calculations provide energy density (energy divided by cell volume) information for intermediate states between one polarity and the other; this is what is plotted in Figure 5 as a function of polarization of the unit cell. These calculations do not attempt to impose any electric field in order to directly represent field-induced polarization reversal; they simply calculate unit cell energy at discrete steps through a stepwise inversion of the polarization. We show through a simple analysis in the supplemental experimental procedures that the individual switching energy pathway can be effectively represented by a collective switching pathway with a single effective barrier ($\omega_{s,c(eff)}$) by equating the volumetric work done (see Figure S4). We demonstrate that the largest switching barrier for the individual mechanism ($\omega_{s,i}$) is a good measure of $\omega_{s,c(eff)}$ and is typically much lower than if the material is constrained to undergo collective switching. Therefore, we can directly compare barriers across different materials—$\omega_{s,i}$ in materials that exhibit individual mechanism and the single barrier in materials that exhibit collective mechanism. We find that the qualitative conclusions, including the materials ranking, are similar whether we use $\omega_{s,i}$ or $\omega_{s,c(eff)}$ as the switching barrier. Figures S5 and S6 show the trends in $\omega_{s,c(eff)}$ (for compounds exhibiting individual mechanism) with E_b and wurtzite c/a, respectively. Figures 2 and 3 are the corresponding trends with $\omega_{s,i}$. Our analysis (see supplemental information) suggests that using $\omega_{s,i}$ to identify candidates is a conservative approach because in most cases, $\omega_{s,i} > \omega_{s,c(eff)}$. This approach is also supported by our recent work on $Al_{1-x}Sc_xN$ alloys, where we show that $\omega_{s,i}$ dependence on the alloy composition determined from SS-NEB calculations is consistent with the experimentally measured trend in coercive field.[33]

Lattice parameters and E_b of alloys

We modeled the $Al_{1-x}Sc_xN$ alloys using 3×3×2 supercells (72 atoms) of the wurtzite AlN primitive cell. For each composition (x), we generated four different disorder configurations by randomly replacing Al with Sc (10 and 13 Al atoms for x = 0.28 and 0.36, respectively). All the supercells were then fully relaxed in the same way as the multinary compounds using GGA+U functional. We report the wurtzite c/a value averaged over the four supercells for each x. To determine the band gap, each supercell was fully relaxed with a hybrid functional (HSE06), and their electronic band structure was calculated on a Γ-centered 2×2×2 k-point grid. The band-gap value used in the E_b calculation is the average over four different disorder configurations. With the averaged band gap, we used the same phenomenological model (Equation 1) to calculate E_b, assuming the same maximum phonon frequency as AlN.

SUPPLEMENTAL INFORMATION

Supplemental information can be found online at https://doi.org/10.1016/j.matt.2024.02.001.

ACKNOWLEDGMENTS

Support for this work was provided by the National Science Foundation under grant no. DMR-2119281 at the Colorado School of Mines and by the Office of Science (SC), Office of Basic Energy Sciences (BES), as part of an Early Career Award at the National Renewable Energy Laboratory, operated by the Alliance for Sustainable Energy, LLC, for the US Department of Energy (DOE) under contract no. DE-AC36-08GO28308. The work (energy calculations to understand switching mechanism) was also partially supported by the Department of Energy Basic Energy Sciences (BES), with additional support from Advanced Scientific Computing Research (ASCR), under program ERW6548. The research was performed using computational resources sponsored by the Department of Energy's Office of Energy Efficiency and Renewable Energy and located at the NREL. The views expressed in the article do not necessarily represent the views of the DOE or the US government.

AUTHOR CONTRIBUTIONS

Investigation, C.-W.L. (lead), N.U.D. (support), K.Y. (support), G.L.B. (support), A.Z. (support), and P.G. (support); data curation, C.-W.L. (lead), N.U.D. (support), and P.G. (support); writing – original draft, C.-W.L.; writing – editing, N.U.D., K.Y., G.L.B., A.Z., and P.G.; conceptualization, G.L.B. (equal), A.Z. (equal), and P.G. (equal); funding acquisition, G.L.B. (equal) and P.G. (equal); project administration, G.L.B. (equal) and P.G. (equal); supervision, P.G.

DECLARATION OF INTERESTS

The authors declare no competing interests.

Received: July 19, 2023
Revised: November 23, 2023
Accepted: February 5, 2024
Published: February 29, 2024

REFERENCES

1. Masanet, E., Shehabi, A., and Koomey, J. (2013). Characteristics of low-carbon data centres. Nat. Clim. Change *3*, 627–630. https://doi.org/10.1038/nclimate1786.

2. Andrae, A.S.G., and Edler, T. (2015). On Global Electricity Usage of Communication Technology: Trends to 2030. Challenges *6*, 117–157. https://doi.org/10.3390/challe6010117.

3. Masanet, E., Shehabi, A., Lei, N., Smith, S., and Koomey, J. (2020). Recalibrating global data center energy-use estimates. Science *367*, 984–986. https://doi.org/10.1126/science.aba3758.

4. Freitag, C., Berners-Lee, M., Widdicks, K., Knowles, B., Blair, G.S., and Friday, A. (2021). The real climate and transformative impact of ICT: A critique of estimates, trends, and regulations. Patterns *2*, 100340. https://doi.org/10.1016/j.patter.2021.100340.

5. Jones, N. (2018). How to stop data centres from gobbling up the world's electricity. Nature *561*, 163–166. https://doi.org/10.1038/d41586-018-06610-y.

6. Mikolajick, T., Slesazeck, S., Mulaosmanovic, H., Park, M.H., Fichtner, S., Lomenzo, P.D., Hoffmann, M., and Schroeder, U. (2021). Next generation ferroelectric materials for semiconductor process integration and their applications. J. Appl. Phys. *129*, 100901. https://doi.org/10.1063/5.0037617.

7. Mulaosmanovic, H., Chicca, E., Bertele, M., Mikolajick, T., and Slesazeck, S. (2018). Nanoscale *10*, 21755–21763. https://doi.org/10.1039/C8NR07135G.

8. Breyer, E.T., Mulaosmanovic, H., Mikolajick, T., and Slesazeck, S. (2021). Perspective on ferroelectric, hafnium oxide based transistors for digital beyond von-Neumann computing. Appl. Phys. Lett. *118*, 050501. https://doi.org/10.1063/5.0035281.

9. Ielmini, D., and Wong, H.S.P. (2018). Nat. Electron. *1*, 333–343. https://doi.org/10.1038/s41928-018-0092-2.

10. Fichtner, S., Wolff, N., Lofink, F., Kienle, L., and Wagner, B. (2019). AlScN: A III-V semiconductor based ferroelectric. J. Appl. Phys. *125*, 114103. https://doi.org/10.1063/1.5084945.

11. Dreyer, C.E., Janotti, A., Van de Walle, C.G., and Vanderbilt, D. (2016). Correct Implementation of Polarization Constants in Wurtzite Materials and Impact on III-Nitrides. Phys. Rev. X *6*, 021038. https://doi.org/10.1103/PhysRevX.6.021038.

12. Hayden, J., Hossain, M.D., Xiong, Y., Ferri, K., Zhu, W., Imperatore, M.V., Giebink, N., Trolier-McKinstry, S., Dabo, I., and Maria, J.P. (2021). Ferroelectricity in boron-substituted aluminum nitride thin films. Phys. Rev. Mater. *5*, 044412. https://doi.org/10.1103/PhysRevMaterials.5.044412.

13. Drury, D., Yazawa, K., Zakutayev, A., Hanrahan, B., and Brennecka, G. (2022). High-Temperature Ferroelectric Behavior of $Al_{0.7}Sc_{0.3}N$. Micromachines *13*, 887. https://doi.org/10.3390/mi13060887.

14. Wolff, N., Islam, M.R., Kirste, L., Fichtner, S., Lofink, F., Žukauskaitė, A., and Kienle, L. (2022). $Al_{1-x}Sc_xN$ Thin Films at High Temperatures: Sc-Dependent Instability and Anomalous Thermal Expansion. Micromachines *13*, 1282. https://doi.org/10.3390/mi13081282.

15. Guido, R., Lomenzo, P.D., Islam, M.R., Wolff, N., Gremmel, M., Schönweger, G., Kohlstedt, H., Kienle, L., Mikolajick, T., Fichtner, S., and Schroeder, U. (2023). Thermal Stability of the Ferroelectric Properties in 100 nm-Thick $Al_{0.72}Sc_{0.28}N$. ACS Appl. Mater. Interfaces *15*,

7030–7043. https://doi.org/10.1021/acsami.2c18313.

16. Liu, X., Ting, J., He, Y., Fiagbenu, M.M.A., Zheng, J., Wang, D., Frost, J., Musavigharavi, P., Esteves, G., Kisslinger, K., et al. (2022). Reconfigurable Compute-In-Memory on Field-Programmable Ferroelectric Diodes. Nano Lett. *22*, 7690–7698. https://doi.org/10.1021/acs.nanolett.2c03169.

17. Kim, K.H., Karpov, I., Olsson, R.H., and Jariwala, D. (2023). Wurtzite and fluorite ferroelectric materials for electronic memory. Nat. Nanotechnol. *18*, 422–441. https://doi.org/10.1038/s41565-023-01361-y.

18. Moriwake, H., Yokoi, R., Taguchi, A., Ogawa, T., Fisher, C.A.J., Kuwabara, A., Sato, Y., Shimizu, T., Hamasaki, Y., Takashima, H., and Itoh, M. (2020). A computational search for wurtzite-structured ferroelectrics with low coercive voltages. Apl. Mater. *8*, 121102. https://doi.org/10.1063/5.0023626.

19. Yasuoka, S., Shimizu, T., Tateyama, A., Uehara, M., Yamada, H., Akiyama, M., Hiranaga, Y., Cho, Y., and Funakubo, H. (2020). Effects of deposition conditions on the ferroelectric properties of (Al1−xScx)N thin films. J. Appl. Phys. *128*, 114103. https://doi.org/10.1063/5.0015281.

20. Wang, P., Wang, D., Vu, N.M., Chiang, T., Heron, J.T., and Mi, Z. (2021). Fully epitaxial ferroelectric ScAlN grown by molecular beam epitaxy. Appl. Phys. Lett. *118*, 223504. https://doi.org/10.1063/5.0054539.

21. Yazawa, K., Mangum, J.S., Gorai, P., Brennecka, G.L., and Zakutayev, A. (2022). Local chemical origin of ferroelectric behavior in wurtzite nitrides. J. Mater. Chem. C *10*, 17557–17566. https://doi.org/10.1039/D2TC02682A.

22. Yazawa, K., Drury, D., Zakutayev, A., and Brennecka, G.L. (2021). Reduced coercive field in epitaxial thin film of ferroelectric wurtzite Al0.7Sc0.3N. Appl. Phys. Lett. *118*, 162903. https://doi.org/10.1063/5.0043613.

23. Zheng, J.X., Fiagbenu, M.M.A., Esteves, G., Musavigharavi, P., Gunda, A., Jariwala, D., Stach, E.A., and Olsson, R.H. (2023). Ferroelectric behavior of sputter deposited Al0.72Sc0.28N approaching 5 nm thickness. Appl. Phys. Lett. *122*, 222901. https://doi.org/10.1063/5.0147224.

24. Zhu, W., Hayden, J., He, F., Yang, J.I., Tipsawat, P., Hossain, M.D., Maria, J.P., and Trolier-McKinstry, S. (2021). Strongly temperature dependent ferroelectric switching in AlN, Al1-xScxN, and Al1-xBxN thin films. Appl. Phys. Lett. *119*, 062901. https://doi.org/10.1063/5.0057869.

25. Dai, Y., and Wu, M. (2023). Covalent-like bondings and abnormal formation of ferroelectric structures in binary ionic salts. Sci. Adv. *9*, eadf8706. https://doi.org/10.1126/sciadv.adf8706.

26. Tagantsev, A.K., Stolichnov, I., Setter, N., Cross, J.S., and Tsukada, M. (2002). Non-Kolmogorov-Avrami switching kinetics in ferroelectric thin films. Phys. Rev. B *66*, 214109. https://doi.org/10.1103/PhysRevB.66.214109.

27. Zhukov, S., Genenko, Y.A., Hirsch, O., Glaum, J., Granzow, T., and von Seggern, H. (2010). Dynamics of polarization reversal in virgin and fatigued ferroelectric ceramics by inhomogeneous field mechanism. Phys. Rev. B *82*, 014109. https://doi.org/10.1103/PhysRevB.82.014109.

28. Tasnádi, F., Alling, B., Höglund, C., Wingqvist, G., Birch, J., Hultman, L., and Abrikosov, I.A. (2010). Origin of the anomalous piezoelectric response in wurtzite Sc(x)Al(1-x)N alloys. Phys. Rev. Lett. *104*, 137601. https://doi.org/10.1103/PhysRevLett.104.137601.

29. Moriwake, H., Konishi, A., Ogawa, T., Fujimura, K., Fisher, C.A.J., Kuwabara, A., Shimizu, T., Yasui, S., and Itoh, M. (2014). Ferroelectricity in wurtzite structure simple chalcogenide. Appl. Phys. Lett. *104*, 242909. https://doi.org/10.1063/1.4884596.

30. Konishi, A., Ogawa, T., Fisher, C.A.J., Kuwabara, A., Shimizu, T., Yasui, S., Itoh, M., and Moriwake, H. (2016). Mechanism of polarization switching in wurtzite-structured zinc oxide thin films. Appl. Phys. Lett. *109*, 102903. https://doi.org/10.1063/1.4962440.

31. Lines, M.E., and Glass, A.M. (2001). Principles and Applications of Ferroelectrics and Related Materials (Oxford University Press).

32. Wang, H., Adamski, N., Mu, S., and Van de Walle, C.G. (2021). Piezoelectric effect and polarization switching in Al1−xScxN. J. Appl. Phys. *130*, 104101. https://doi.org/10.1063/5.0056485.

33. Lee, C.W., Yazawa, K., Zakutayev, A., Brennecka, G.L., and Gorai, P. (2023). Switching it up: New Mechanisms Revealed in Wurtzite-type Ferroelectrics. https://doi.org/10.26434/chemrxiv-2023-xdp95.

34. Sun, W., Bartel, C.J., Arca, E., Bauers, S.R., Matthews, B., Orvañanos, B., Chen, B.R., Toney, M.F., Schelhas, L.T., Tumas, W., et al. (2019). A map of the inorganic ternary metal nitrides. Nat. Mater. *18*, 732–739. https://doi.org/10.1038/s41563-019-0396-2.

35. Ferri, K., Bachu, S., Zhu, W., Imperatore, M., Hayden, J., Alem, N., Giebink, N., Trolier-McKinstry, S., and Maria, J.P. (2021). Ferroelectrics everywhere: Ferroelectricity in magnesium substituted zinc oxide thin films. J. Appl. Phys. *130*, 044101. https://doi.org/10.1063/5.0053755.

36. Zeilinger, M., Kurylyshyn, I.M., Häussermann, U., and Fässler, T.F. (2013). Revision of the Li–Si Phase Diagram: Discovery and Single-Crystal X-ray Structure Determination of the High-Temperature Phase $Li_{4.11}Si$. Chem. Mater. *25*, 4623–4632. https://doi.org/10.1021/cm4029885.

37. Breternitz, J., and Schorr, S. (2021). Symmetry relations in wurtzite nitrides and oxide nitrides and the curious case of $Pmc2_1$. Acta Crystallogr. A *77*, 208–216. https://doi.org/10.1107/S2053273320015971.

38. Biswas, B., and Saha, B. (2019). Development of semiconducting ScN. Phys. Rev. Mater. *3*, 020301. https://doi.org/10.1103/PhysRevMaterials.3.020301.

39. Yazawa, K., Hayden, J., Maria, J.P., Zhu, W., Trolier-McKinstry, S., Zakutayev, A., and Brennecka, G.L. (2023). Anomalously abrupt switching of wurtzite-structured ferroelectrics: simultaneous non-linear nucleation and growth model. Mater. Horiz. advance article. https://doi.org/10.1039/D3MH00365E.

40. Liu, Z., Wang, X., Ma, X., Yang, Y., and Wu, D. (2023). Doping effects on the ferroelectric properties of wurtzite nitrides. Appl. Phys. Lett. *122*, 122901. https://doi.org/10.1063/5.0145818.

41. Calderon, S., Hayden, J., Baksa, S.M., Tzou, W., Trolier-McKinstry, S., Dabo, I., Maria, J.P., and Dickey, E.C. (2023). Atomic-scale polarization switching in wurtzite ferroelectrics. Science *380*, 1034–1038. https://doi.org/10.1126/science.adh7670.

42. https://github.com/prashungorai/papers/tree/main/2023/FEsearch.

43. Kruse, M., Petralanda, U., Gjerding, M.N., Jacobsen, K.W., Thygesen, K.S., and Olsen, T. (2023). Two-dimensional ferroelectrics from high throughput computational screening. Comput. Mater. *9*, 45. https://doi.org/10.1038/s41524-023-00999-5.

44. Zhang, X.L., Chen, Z.X., Cross, L.E., and Schulze, W.A. (1983). Dielectric and piezoelectric properties of modified lead titanate zirconate ceramics from 4.2 to 300 K. J. Mater. Sci. *18*, 968–972. https://doi.org/10.1007/BF00551962.

45. Sun, Y., Boggs, S.A., and Ramprasad, R. (2012). The intrinsic electrical breakdown strength of insulators from first principles. Appl. Phys. Lett. *101*, 132906. https://doi.org/10.1063/1.4755841.

46. Gorai, P., Krasikov, D., Grover, S., Xiong, G., Metzger, W.K., and Stevanović, V. (2023). A search for new back contacts for CdTe solar cells. Sci. Adv. *9*, eade3761. https://doi.org/10.1126/sciadv.ade3761.

47. Zakutayev, A., Bauers, S.R., and Lany, S. (2022). Experimental Synthesis of Theoretically Predicted Multivalent Ternary Nitride Materials. Chem. Mater. *34*, 1418–1438. https://doi.org/10.1021/acs.chemmater.1c03014.

48. NREL Materials Database materials.nrel.gov

49. Kresse, G., and Furthmüller, J. (1996). Efficient iterative schemes for ab initio total-energy calculations using a plane-wave basis set. Phys. Rev. B *54*, 11169–11186. https://doi.org/10.1103/PhysRevB.54.11169.

50. Perdew, J.P., Burke, K., and Ernzerhof, M. (1996). Generalized Gradient Approximation Made Simple. Phys. Rev. Lett. *77*, 3865–3868. https://doi.org/10.1103/PhysRevLett.77.3865.

51. Stevanović, V., Lany, S., Zhang, X., and Zunger, A. (2012). Correcting density functional theory for accurate predictions of compound enthalpies of formation: Fitted elemental-phase reference energies. Phys. Rev. B *85*, 115104. https://doi.org/10.1103/PhysRevB.85.115104.

52. Kim, C., Pilania, G., and R. (2016). From Organized High-Throughput Data to Phenomenological Theory using Machine Learning: The Example of Dielectric Breakdown. Chem. Mater. *28*, 1304–1311. https://doi.org/10.1021/acs.chemmater.5b04109.

53. Sheppard, D., Xiao, P., Chemelewski, W., Johnson, D.D., and Henkelman, G. (2012). A

generalized solid-state nudged elastic band method. J. Chem. Phys. *136*, 074103. https://doi.org/10.1063/1.3684549.

54. Krukau, A.V., Vydrov, O.A., Izmaylov, A.F., and Scuseria, G.E. (2006). Influence of the exchange screening parameter on the performance of screened hybrid functionals. J. Chem. Phys. *125*, 224106. https://doi.org/10.1063/1.2404663.

55. King-Smith, R.D., and Vanderbilt, D. (1993). Theory of polarization of crystalline solids. Phys. Rev. B *47*, 1651–1654. https://doi.org/10.1103/PhysRevB.47.1651.

56. Resta, R. (1994). Macroscopic polarization in crystalline dielectrics: the geometric phase approach. Rev. Mod. Phys. *66*, 899–915. https://doi.org/10.1103/RevModPhys.66.899.

57. Smidt, T.E., Mack, S.A., Reyes-Lillo, S.E., Jain, A., and Neaton, J.B. (2020). Sci. Data *7*, 72. https://doi.org/10.1038/s41597-020-0407-9.

58. Henkelman, G., Uberuaga, B.P., and Jónsson, H. (2000). A climbing image nudged elastic band method for finding saddle points and minimum energy paths. J. Chem. Phys. *113*, 9901–9904. https://doi.org/10.1063/1.1329672.